NASA/TM—2012-217245 ISABE–2011–1106

Investigations of a Combustor Using a 9-Point Swirl-Venturi Fuel Injector: Recent Experimental Results

Yolanda R. Hicks, Christopher M. Heath, Robert C. Anderson, and Kathleen M. Tacina
Glenn Research Center, Cleveland, Ohio

April 2012

NASA STI Program . . . in Profile

Since its founding, NASA has been dedicated to the advancement of aeronautics and space science. The NASA Scientific and Technical Information (STI) program plays a key part in helping NASA maintain this important role.

The NASA STI Program operates under the auspices of the Agency Chief Information Officer. It collects, organizes, provides for archiving, and disseminates NASA's STI. The NASA STI program provides access to the NASA Aeronautics and Space Database and its public interface, the NASA Technical Reports Server, thus providing one of the largest collections of aeronautical and space science STI in the world. Results are published in both non-NASA channels and by NASA in the NASA STI Report Series, which includes the following report types:

- TECHNICAL PUBLICATION. Reports of completed research or a major significant phase of research that present the results of NASA programs and include extensive data or theoretical analysis. Includes compilations of significant scientific and technical data and information deemed to be of continuing reference value. NASA counterpart of peer-reviewed formal professional papers but has less stringent limitations on manuscript length and extent of graphic presentations.

- TECHNICAL MEMORANDUM. Scientific and technical findings that are preliminary or of specialized interest, e.g., quick release reports, working papers, and bibliographies that contain minimal annotation. Does not contain extensive analysis.

- CONTRACTOR REPORT. Scientific and technical findings by NASA-sponsored contractors and grantees.

- CONFERENCE PUBLICATION. Collected papers from scientific and technical conferences, symposia, seminars, or other meetings sponsored or cosponsored by NASA.

- SPECIAL PUBLICATION. Scientific, technical, or historical information from NASA programs, projects, and missions, often concerned with subjects having substantial public interest.

- TECHNICAL TRANSLATION. English-language translations of foreign scientific and technical material pertinent to NASA's mission.

Specialized services also include creating custom thesauri, building customized databases, organizing and publishing research results.

For more information about the NASA STI program, see the following:

- Access the NASA STI program home page at *http://www.sti.nasa.gov*

- E-mail your question via the Internet to *help@sti.nasa.gov*

- Fax your question to the NASA STI Help Desk at 443–757–5803

- Telephone the NASA STI Help Desk at 443–757–5802

- Write to:
  NASA Center for AeroSpace Information (CASI)
  7115 Standard Drive
  Hanover, MD 21076–1320

NASA/TM—2012-217245 ISABE–2011–1106

Investigations of a Combustor Using a 9-Point Swirl-Venturi Fuel Injector: Recent Experimental Results

Yolanda R. Hicks, Christopher M. Heath, Robert C. Anderson, and Kathleen M. Tacina
Glenn Research Center, Cleveland, Ohio

Prepared for the
20th International Symposium on Air Breathing Engines (ISABE 2011)
sponsored by the International Society for Air Breathing Engines
Göteborg, Sweden, September 12–16, 2011

National Aeronautics and
Space Administration

Glenn Research Center
Cleveland, Ohio 44135

April 2012

Acknowledgments

This work was supported by the Subsonic Fixed Wing and Supersonics Projects in NASA's Aeronautics Research Mission Directorate. The authors gratefully acknowledge Changlie Wey for his assistance and guidance. We also thank the CE-5 test crew, especially our technicians Jeff Hamman, Bill Rozman, and Harold Redloske.

This work was sponsored by the Fundamental Aeronautics Program at the NASA Glenn Research Center.

Level of Review: This material has been technically reviewed by technical management.

Available from

NASA Center for Aerospace Information
7115 Standard Drive
Hanover, MD 21076–1320

National Technical Information Service
5301 Shawnee Road
Alexandria, VA 22312

Available electronically at http://www.sti.nasa.gov

Investigations of a Combustor Using a 9-Point Swirl-Venturi Fuel Injector: Recent Experimental Results

Yolanda R. Hicks, Christopher M. Heath, Robert C. Anderson, and Kathleen M. Tacina
National Aeronautics and Space Administration
Glenn Research Center
Cleveland, Ohio 44135

Abstract

This paper explores recent results obtained during testing in an optically-accessible, JP8-fueled, flame tube combustor using baseline Lean Direct Injection (LDI) research hardware. The baseline LDI geometry has nine fuel/air mixers arranged in a 3 × 3 array. Results from this nine-element array include images of fuel and OH speciation via Planar Laser-Induced Fluorescence (PLIF), which describe fuel spray pattern and reaction zones. Preliminary combustion temperatures derived from Stokes/Anti-Stokes Spontaneous Raman Spectroscopy are also presented. Other results using chemiluminescence from major combustion radicals such as CH^* and C_2^* serve to identify the primary reaction zone, while OH PLIF shows the extent of reaction further downstream. Air and fuel velocities and fuel drop size results are also reported.

Nomenclature

Symbols

A_f, m^2	combustor cross-sectional area
A_e, m^2	effective mixer exit area
C_2^*,	diatomic carbon radical
CH^*	CH radical
D_{32}, μm	Sauter mean diameter
f, mm	focal length
L/D	length-to-diameter ratio
OH^*	hydroxyl radical
NO_x	oxides of nitrogen
P, kPa	pressure
P_3, kPa	inlet combustor pressure
T, K	temperature
T_3, K	inlet combustor temperature
T_{ad}, K	adiabatic flame temperature
U, m/s	axial velocity component
V, m/s	transverse velocity component
W, m/s	vertical velocity component
X	axial flow direction
Y	transverse flow direction
Z	vertical flow direction
ΔP/P	combustor pressure drop
Φ	equivalence ratio

Abbreviations

AS	Anti-Stokes
CFD	Computational Fluid Dynamics

FWHM	Full Width Half Maximum
(I)CCD	(Intensified) Charge-Coupled Device
LDI	Lean Direct Injection
LDV	Laser Doppler Velocimetry
NASA	National Aeronautics and Space Administration
Nd:YAG	Neodymium: Yttrium Aluminum Garnet
PLIF	Planar Laser-Induced Fluorescence
PDI	Phase Doppler Interferometry
PIV	Particle Image Velocimetry
RMS	Root Mean Square
S	Stokes
SRS	Spontaneous Raman Scattering
UHCs	Unburned Hydrocarbons
UV	Ultraviolet

Introduction

The International Civil Aviation Organization estimates that aviation accounts for nearly two percent of the anthropogenic-induced carbon dioxide emissions global wide and contributes 3 percent to the potential warming effect (Ref. 1). Those numbers are expected to increase an additional 1 to 2 percent by 2050 (Ref. 1). Near the primary flight corridors of the globe, the effects from aviation can become more severe. At ground level, NO_x increase the production of ozone, leading to smog. Estimates are that commercial aircraft operations generate 0.4 percent of all national low-altitude NO_x emissions (below 913-m) (Ref. 2). From a survey released in 2005, the Federal Aviation Administration (FAA) estimates airports contribute between 0.7 to 6.1 percent to the NO_x inventory of the surrounding locality (Ref. 3). In the troposphere, NO_x have been found to increase ozone production. At stratospheric altitudes for supersonic cruise, NO_x have been shown to play a reverse effect and decrease the protective ozone layer (Ref. 4).

To reduce the environmental effects of aviation and ensure that aircraft gas turbines meet future more stringent noise and emissions regulations, NASA is developing engine technologies that will decrease emissions while simultaneously increasing fuel efficiency. However, many technologies that increase engine efficiency also increase temperature and pressure at the inlet of the combustor, T_3 and P_3; for a given combustor technology, increasing T_3 and P_3 often increase NO_x emissions. NASA has investigated several combustion concepts to reduce NO_x emissions. This paper describes optical measurements from one low NO_x combustor concept: lean direct injection.

As the name implies, in LDI the combustor operates fuel-lean without a rich front end: all of the combustor air except that used for liner cooling enters through the combustor dome (Ref. 5). Like other lean burn combustor concepts, LDI reduces NO_x by minimizing flame temperature; in fuel lean combustion, NO_x is an exponential function of temperature. To eliminate local “hot spots” that produce high levels of NO_x, lean burn combustion concepts rely on the fuel and air being well-mixed before burning occurs. Thus, LDI requires rapid fuel vaporization and fuel-air mixing. LDI achieves this by using a multi-element concept in which several small fuel/air mixers replace a single conventional fuel/air mixer.

Improved understanding of LDI operation will permit guideline development for future LDI combustor refinement. In order to achieve this understanding, examination of the physical and chemical processes that occur is required. The required information can be provided either by computational fluid dynamics (CFD) or by detailed optical measurements. In any case, detailed optical measurements are required because CFD results also require validation.

Optical measurements that have been applied to flows in simulated gas turbine combustors include Planar Laser-Induced Fluorescence (PLIF), Planar Elastic Scattering, Spontaneous Raman Spectroscopy (SRS), Phase Doppler Interferometry (PDI), and Particle Image Velocimetry (PIV) (Refs. 6 to 10).

Results of those measurements include combustion species maps, velocities, fuel/air ratios, and turbine profile factors. These measurements are used to study fuel injection, mixedness, and combustion processes and are part of a database of measurements that will be used for validating computational combustion models (Refs. 11 to 15).

This paper presents additional measurements for a nine-element LDI array. Measurements include high speed imaging, flame spectra, velocity, and turbulence. The data were collected over a range of inlet conditions that simulate the conditions of next-generation aircraft combustors. Results that compare fueling all nine elements with fueling only the center element are presented here for the first time.

Experimental Setup

The LDI hardware was tested in a high temperature and high pressure flame tube combustor rig with partial optical access directly downstream of the fuel injection site. The experimental facility and instrumentation offered the ability to perform non-intrusive optical and laser-based diagnostics, to examine fluid and chemical processes during combustion. The test cell was capable of supplying non-vitiated inlet air to the combustor at temperatures between 505 and 866 K, pressures between 1034- and 1724-kPa with flow rates up to 4.54 kg/s.

An isolated full-section view of the window assembly and downstream flame tube are displayed in Figure 1. The combustor housing is 74-cm in length and lined with an aluminum oxide ceramic to withstand average temperatures reaching 2033 K. UV-grade fused silica windows (38.1- by 50.8-mm) are mounted just downstream of the fuel injection site and provide optical access from three sides of the square combustion chamber. The combustion chamber cross-section measures 76.2- by 76.2-mm. The bottom of the chamber is reserved for a spark igniter and provides no physical or optical access. The grade of quartz used in the windows offers a light transmission of at least 80 percent within a spectral range from 180- to 3300-nm. Nitrogen film cooling is used internally to regulate window temperature and accounts for no more than 10 percent by mass of the total inlet air flow.

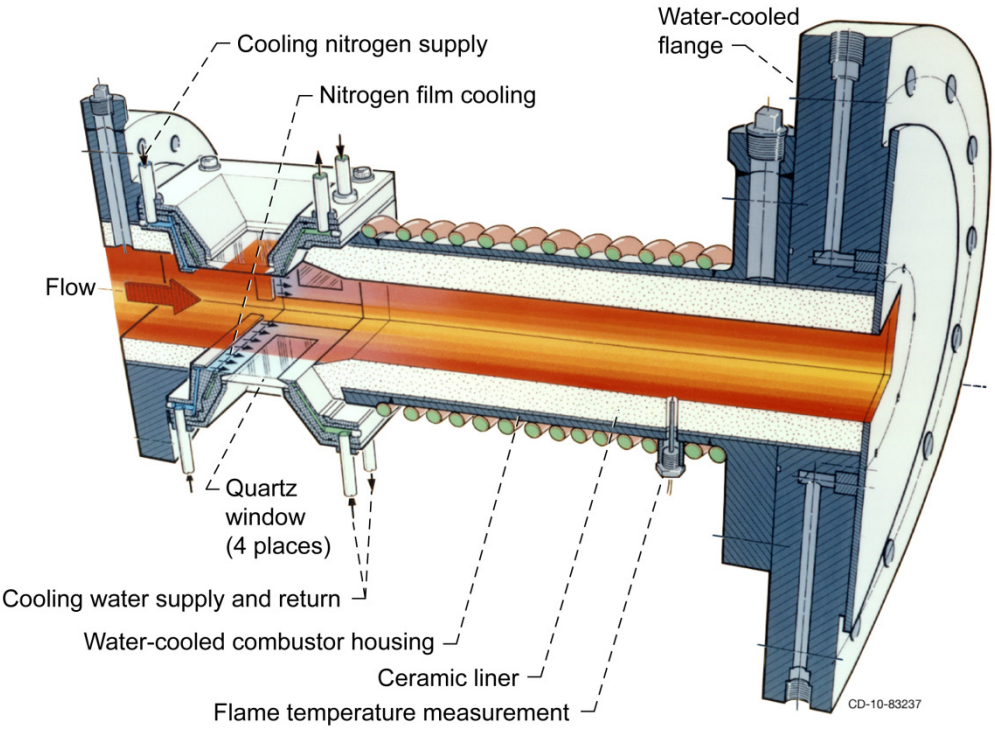

Figure 1.—Illustration of flame tube and window housings.

The baseline 9-point LDI test hardware is described in Tacina et al. (Ref. 5) and consists of a 3 × 3 injector array measuring 76.2- by 76.2-mm with injectors spaced 25.4-mm (center-to-center). Each injector element is comprised of a set of six helical, axial vanes angled at 60° that surround a simplex nozzle designed to produce a hollow cone fuel spray. The nozzle atomizes and injects liquid fuel (Jet-A, JP-8) at the throat of a converging-diverging venturi. The calculated swirl number for this injector architecture is 1.0. A schematic of a single injector element is displayed in the cut-away view of Figure 2. An end-view of the full 9-point array is shown in Figure 3.

The optical instrumentation was fixed to a set of stages to provide traversing ability along up to three orthogonal directions. In this work X- is defined as the axial stream-wise direction, with X = 0-mm being the exit (dump) plane of the 9-point LDI hardware. Y- is the transverse horizontal direction and Z- is the vertical direction, with (Y = 0-mm, Z = 0-mm) at the center of the center injector. Positive directions follow from the right-hand-rule, with positive X downstream and Z up.

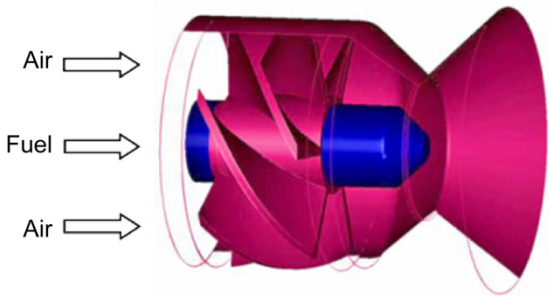

Figure 2.—Schematic drawing that shows the relative spatial positioning of the air swirler, fuel nozzle, and venturi for each injector element.

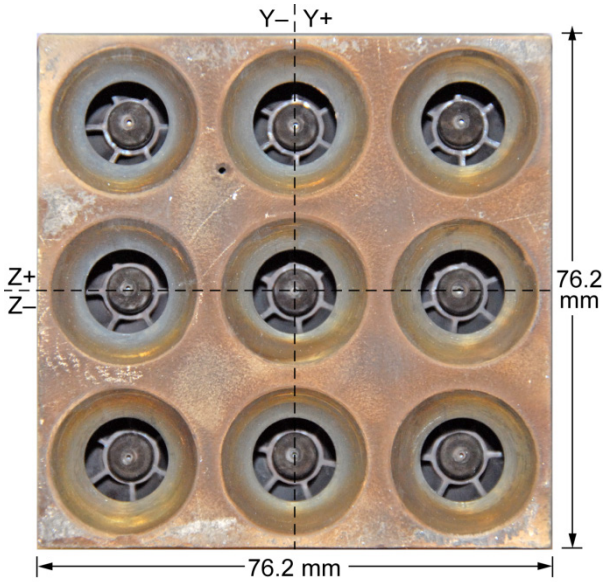

Figure 3.—End view of the 9-point LDI test hardware.

Diagnostic Setup

Imaging Techniques—PLIF, Luminescence, PIV

The experimental setups that fall under the category of imaging techniques were similar in that any light scattered or emitted was collected, using an imaging array (camera), from an angle perpendicular to the combustor flow direction, as illustrated in Figure 4. Various filters were applied so that only the wavelength bands of interest were allowed to pass to the detector. For PIV and PLIF, the two 2–D techniques that use lasers, the laser beam was formed into a light sheet using a set of cylindrical lenses. The sheet was passed vertically through the test section and aligned parallel with the flow direction. For these methods, the laser sheet and collection optics were traversed together so as to maintain focus on the laser sheet. For chemiluminescence measurements, either species-specific, or high speed imaging, the camera was positioned so that the vertical center plane of the test rig was in focus.

OH and fuel PLIF images, along with chemiluminescence images of C_2, and CH, were obtained using the same receiving optics and camera. Collection optics included the appropriate filter (FWHM of 10-nm, typical) attached to a UV-grade, f = 105-mm, f/4.5, macro camera lens. The light was collected using a gated, 16-bit, 1k × 1k pixel array, intensified CCD (ICCD) camera having a Gen II Super-Blue-Slow-Gate intensifier. The gate time used was 50-ns. For PLIF, OH and fuel molecules were excited using a 10-Hz, frequency-doubled Nd:YAG-pumped dye laser/frequency mixer system to achieve wavelengths around 282-nm. The laser was formed into a sheet using a pair of cylindrical lenses, to obtain a sheet approximately 300 μm thick. For PLIF, we used on-chip averages of 200 gates, and traversed across the flow along the Y axis in 1-mm increments. For chemiluminescence, we averaged 600 gates on-chip. The filters used to isolate the species were 313-nm (OH), 334-nm (fuel), 430-nm (CH), and 515-nm (C_2).

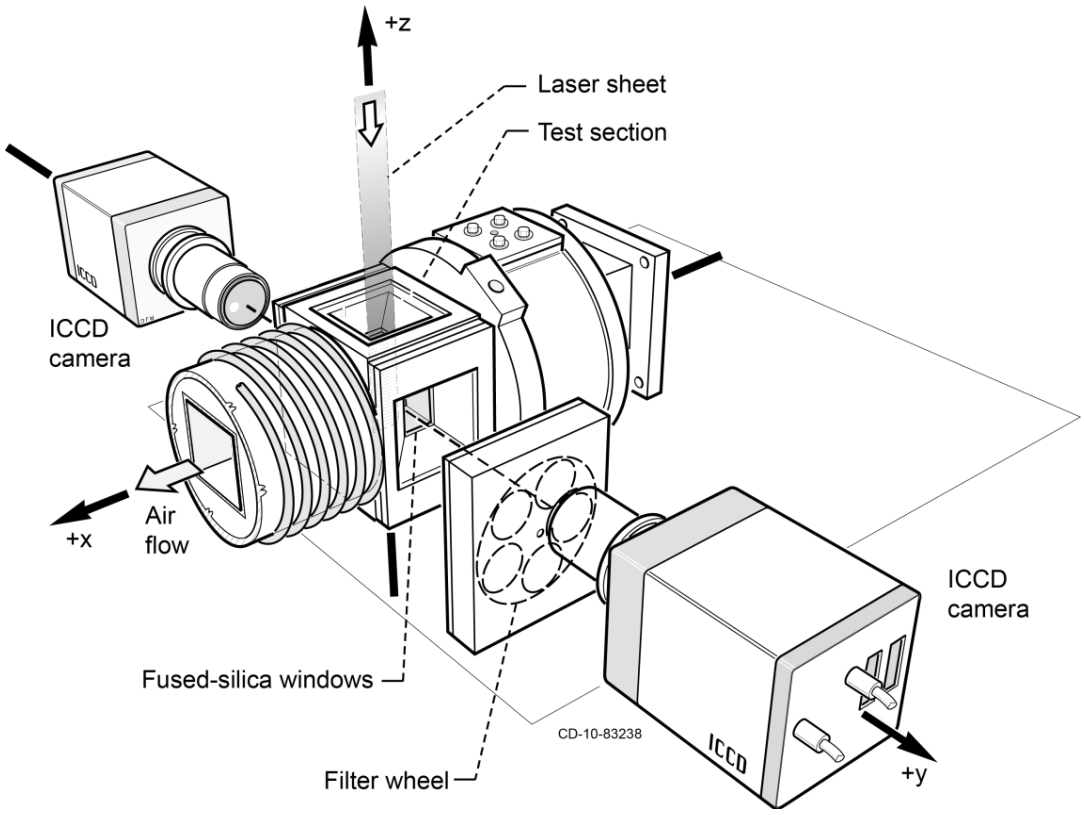

Figure 4.—Illustration that shows a typical 2–D or 1–D imaging arrangement such as for PLIF or PIV.

Flame imaging was achieved using a 12-bit, high speed CMOS camera (1k × 1k) focused on the vertical center plane. Light emitted from the volume and within the field-of-view of the collection optics was collected. In the work presented here, we used a frame rate of 10,000 frames per second, image exposure time of 40-μs, and image resolution of 576 × 944 pixels. The flame chemiluminescence was collected using an f = 150-mm, f/1.2 lens. The camera array was sensitive to visible light; the light collected was largely a combination of CH and C_2 emissions.

The PIV data were acquired using a 15-Hz double-head, frequency-doubled, Nd:YAG laser and a single, interline transfer, CCD camera. For the un-fueled, air-only tests, 0.7-μm diameter alumina particles were seeded into the air inlet plenum 10-L/D before the plenum exit. The inlet plenum feeds the flow to the flame tube test section. For combusting experiments, seed was not used. Instead, we collected the light scattered by fuel particles to measure the liquid phase velocity. We used a mechanical leaf shutter to block light from the luminescent flame.

Imaging Techniques—Raman Scattering

As with the 2–D imaging above, 1–D Spontaneous (Vibrational) Raman Scattering (SRS) was collected 90° from the incoming light and square to the test rig. We used a 30-Hz, frequency-doubled, Nd:YAG laser focused using a spherical lens into the test section. The beam waist at the focus was approximately 2-mm. Collection of the Raman-scattered light was achieved using an f = 60-mm, f/2.8, macro lens to 0.22NA, 37 fiber linear array. Each fiber is 200-mm in diameter. The light collected passed through a notch filter, and focused onto the slit of an f = 300-mm spectrometer. The slit was set full open, to 1-mm. The light was dispersed using a 300 groove/mm grating blazed at 500-nm. The light was collected using an intensified CCD camera (1k × 1k pixel array, 18-mm, Gen III, Super Blue intensifier). Each data file was comprised of 1005 laser shots, acquired using a combination of 30 shots on-chip with 67 software accumulations. The combination of input and receiving optics used resulted in a probe volume approximately 2.6-mm high, 2-mm diameter, and positioned 4.4-mm above the rig centerline. The system was traversed horizontally in 5-mm increments both in X- and Y- directions.

Phase Doppler Interferometry

Three component Phase Doppler Interferometry (PDI) measurements were performed using a setup similar to that displayed in Figure 5 where transmitter and receiver optics were arranged in a 30° off-axis forward scatter configuration, with both transmitter and receiver oriented 15° with respect to the combustor Y- planes.

An argon-ion laser was used to generate a green (514.5-nm), blue (488-nm) and violet (476.5-nm) beam pair. Due to limited optical access, the three-color PDI system used a single optical head to transmit the beam pairs that intersected at the measurement volume. As shown in Figure 5, the beams did not provide orthogonal measurements, so a combined optical and geometric transform of the three measured velocity channels into the rectilinear coordinate system was required.

Data were obtained in a point-wise manner. Focal lengths for both the transmitter and receiver were 500-mm. The measurement volume measured 0.076-mm in diameter by 1.03-mm in length.

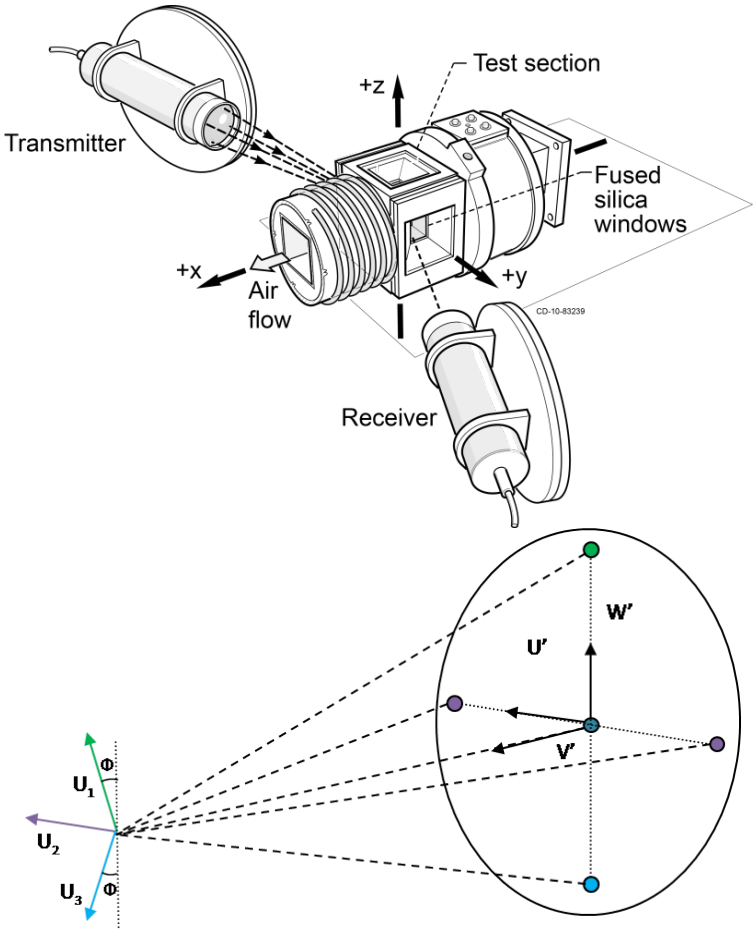

Figure 5.—PDI setup. Top: transmitter-receiver orientation about test rig; Bottom: arrangement of beams transmitted through the transceiver and spatial relation to orthogonal components.

Results and Discussion

In Figure 6 and Figure 7, we present PIV results from the Y=0 plane that help describe the combustor/mixer system air flow. The inlet conditions were T_3 = 828 K and P_3 = 1034-kPa. The time between image pairs was 5-μs, with a pair sample rate of 15-Hz. Figure 6 shows a sequence of ten consecutive "instantaneous" 2–D velocity fields which allows one to see the variation in flow structure. Flow is left to right. Regions in red represent downstream flow and those in blue show upstream motion. Although no two instantaneous fields are alike, we observe similar structures within each. The regions between injectors exhibit high downstream velocity, whereas upstream, near z = 0, negative velocities occur. The average velocity and RMS velocity fields shown in Figure 7, which are the result of averaging 500 instantaneous fields, serve to confirm those observations. The absolute magnitudes of the 2–D velocities are plotted as gray-scale contours, and the direction of fluid motion is given using arrows. The region immediately downstream of the injectors shows upstream motion and the region between the injectors has high downstream velocity. The velocity plot also shows the upstream recirculating eddy regions that exist between the injectors where the upstream and downstream regions shear. The black contour shows the boundaries of zero velocity that separate the central recirculation zones from the bulk downstream motion. The RMS plot shows that the greatest variation in the air velocity occurs in the region between injectors. These features are in agreement with CFD calculations (Ref. 12).

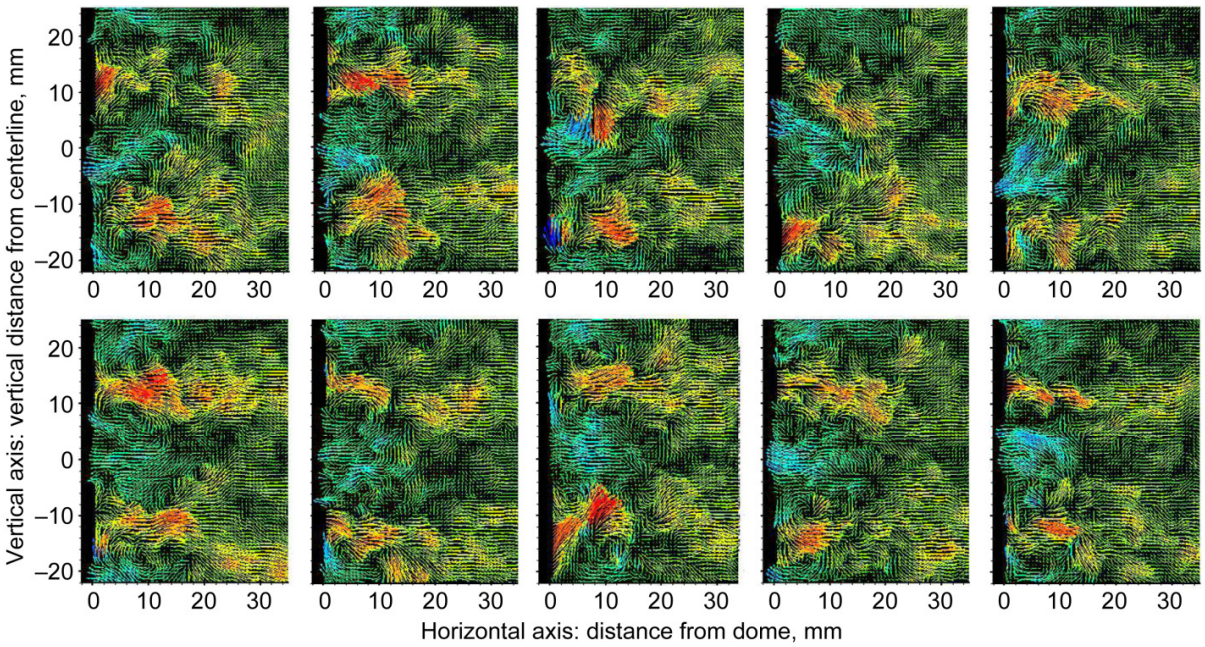

Figure 6.—Ten consecutive instantaneous PIV Axial-Vertical velocity Fields in the vertical center plane. (Y = 0). T_3 = 828 K, P_3 = 1034-kPa. Flow is left to right.

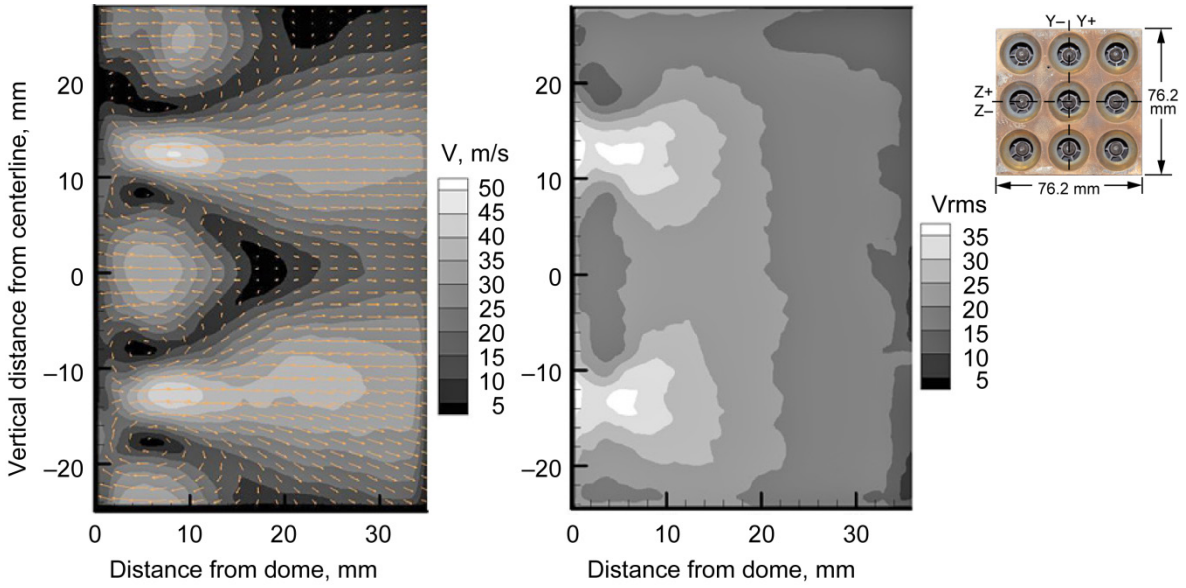

Figure 7.—Average velocity field (left) and RMS of velocity (right) within the vertical center plane, (Y = 0) computed from 500, 2–D image pairs. T_3 = 828 K, P_3 = 1034-kPa. Flow left to right.

Once we added fuel and combustion occurred at this inlet temperature, our PDI measurements indicated that, on average, the fuel droplets were small, with maximum Sauter mean diameter, D_{32}, around 40-µm (Figure 8). The majority of drops were less than 12-µm. Figure 9 shows a result during unseeded combustion acquired using the PDI system at inlet conditions T_3 = 828 K, P_3 = 1379-kPa and ϕ = 0.45. It is an end view at x = 3-mm, with flow coming out of the page that plots the azimuthal velocities for three drop size bins: drops less than 10-µm, greater that 10-µm and less than 20-µm, and droplets greater than 20-µm. From this perspective, one can see that there is rotation approximately about the centerline, which has little to no V-W velocity. The V-W components increase in magnitude with greater distance from the centerline, predominately radially outward. Near the center, most of the vectors are overlapped and present mostly as

axial velocity. Once out near the diffuser circumference, we see some differentiation in velocity, with the larger (heavier) drops lagging in direction (assuming those drops smaller than 10-μm follow the flow). Although the different directions the drops take become distinguishable, there is no obvious pattern that would allow us to say that any one size class moves in a particular manner. The separation does, however, show that the larger drops probably assume more of a ballistic trajectory, with minimal influence from the local air field.

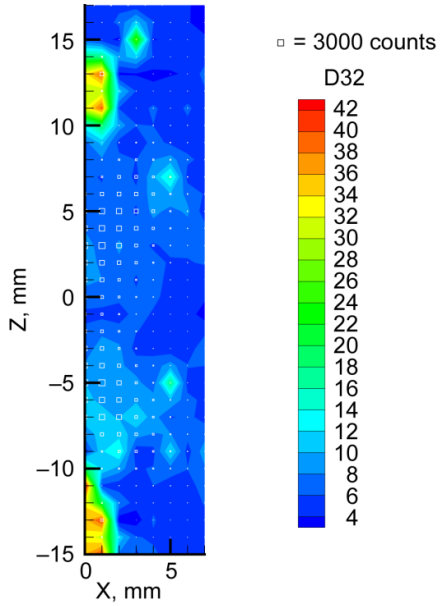

Figure 8.—Plot showing sauter mean diameter within the Y=0 plane. The scatter points represent valid droplet count during 10-sec acquisition time. Inlet conditions: T_3 = 828 K, P_3 = 1034-kPa, ϕ = 0.45. Flow is left to right.

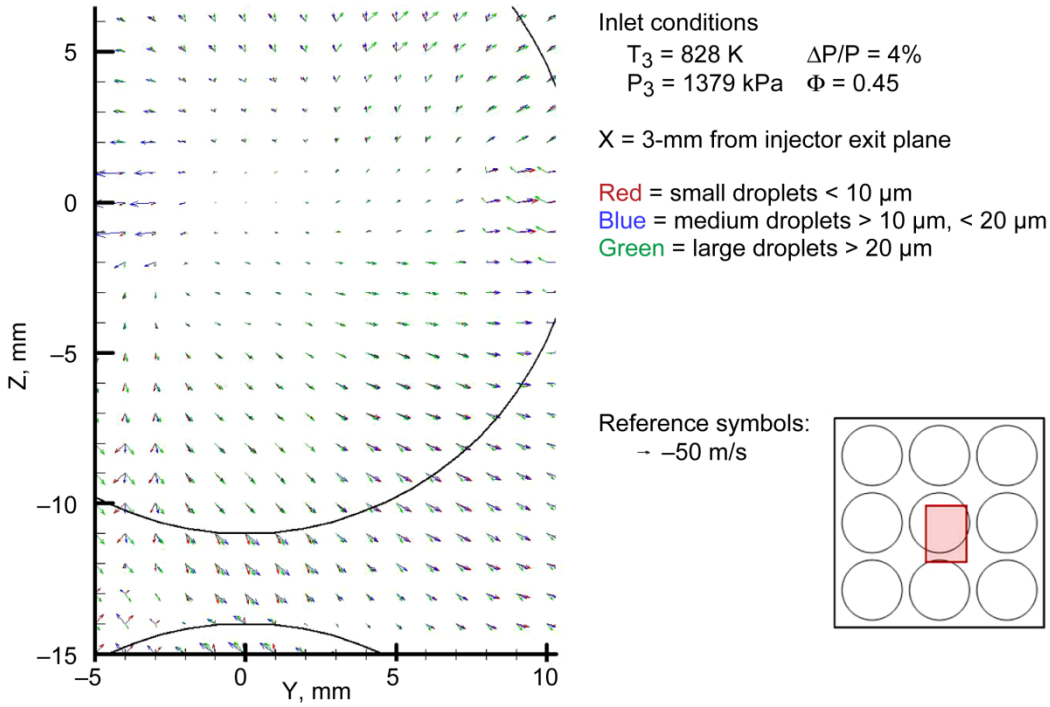

Figure 9.—End view showing azimuthal velocity vectors differentiated by fuel droplet size for three size bins. Inlet conditions: T_3 = 828 K, P_3 = 1379-kPa, ϕ = 0.45. Flow is out of page.

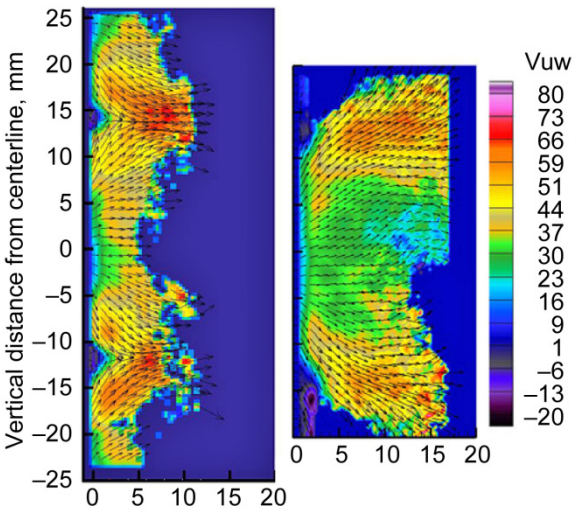

Figure 10.—PIV from fuel drops at Y = 0. T_3 = 617 K, P_3 = 1034-kPa. Left: ϕ = 0.45. Right: ϕ_{loc} = 1.45. Flow is left to right.

The PIV measurements acquired during combustion result from droplet light scatter only; as with the PDI measurements, the flow is unseeded. In the results presented in Figure 10, the combustor pressure is 1034-kPa, and the inlet temperature is 617 K. We used a lower inlet temperature because at 828 K, we did not have many drops from which to scatter. With lower inlet temperatures, there was less fuel vaporization and we were able to acquire images with good contrast and dynamic range for PIV processing.

The two images presented in Figure 10 represent two flow configurations. The left image was acquired with all nine injectors fueled equally, with $\phi_{loc} = \phi_{tot} = 0.45$ (left); the right image was acquired with only the center injector fueled, with $\phi_{loc} = 1.45$ and $\phi_{tot} = 0.16$. They are plotted on the same scale.

For this injector, all the inlet air passes through the dome, so all nine swirlers act upon the air. A lot more fuel passes through the center injector when it operates alone compared to when all nine injectors are fueled; this must be the case in order to maintain stability without the flame blowing out. We find that we can measure farther downstream in the one-injector case partly because there is more fuel in the region to begin with and also because at this low inlet temperature, less fuel has vaporized. Based on the direction of the fluid within the fuel spray cone around the central injector, there is no change in the fuel spray angle; it appears that the presence of adjacent air swirlers helps to confine the fuel spray to the region immediately downstream from its corresponding air swirler element. Expected larger fuel droplets unable to follow the flow also act to confine the fuel mass closer to the exit plane.

We analyzed the flame luminescence images obtained with the ICCD and the high speed camera and present the results in Figure 11 to Figure 14. Figure 11 is a matrix showing the average chemiluminescence signal for CH^* for three inlet temperatures (row-wise) and two fuel staging conditions for a combustor pressure of 1034-kPa. The left and center columns have all injectors equally fueled with equivalence ratios of 0.45 and 0.35; the last column has results with only the center injector fueled. The overall equivalence ratio for the center-only cases is 0.15 or 0.16. Flow is from left to right. The images were obtained by integrating, on-chip, 600 50-ns wide gates (as for PLIF), for a total exposure of 30-µs over the 1 minute data acquisition time. The images shown are auto-scaled to highlight their structural features.

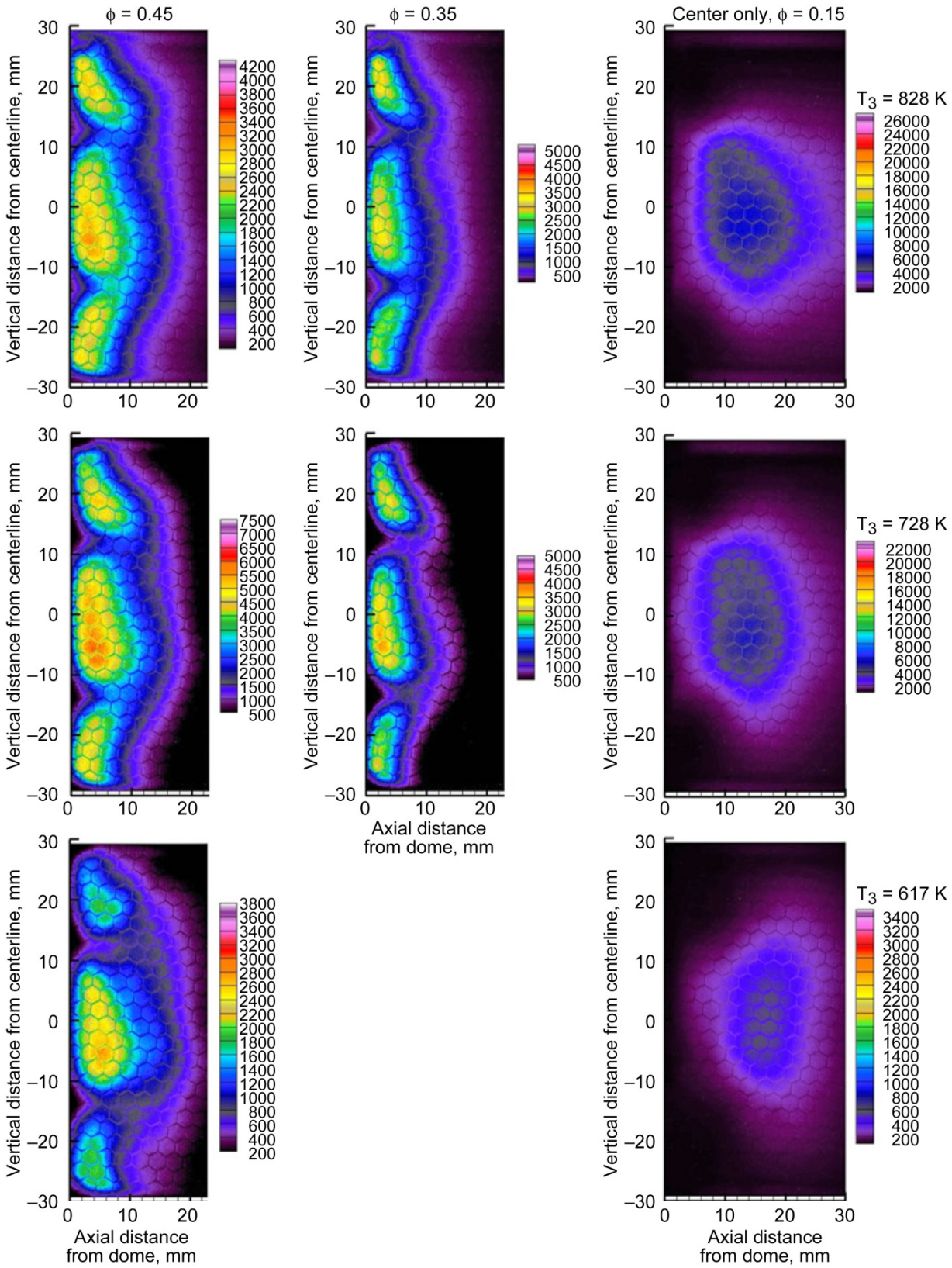

Figure 11.—On-chip integrated averages of CH^* at various inlet conditions. Rows (top to bottom): T_3 = 828, 728, 617 K. Columns (L-M): ϕ = 0.45, 0.35 Right column, center-only fueled. Flow is left to right.

The extent of signal downstream follows from the amount of fuel that flows from a given injector. For example, in considering the center injector row for the 828 K inlet temperature, the CH^* signal extends from X = 10-mm (ϕ_{loc} = 0.35) to X = 16-mm (ϕ_{loc} = 0.45) to X = 20-mm (ϕ_{loc} = 1.32). For center-only fueling, as well, we note a delay in the onset of chemical activity, i.e., the flame front sits farther downstream from the dome than with the corresponding all-fueled conditions. Regardless of fueling, we also observe an upstream shift in the location of peak signal intensity with increase in inlet temperature.

Figure 12 shows statistical results of processing 9001 consecutive flame luminosity images acquired at 10-kHz, and is typical of all high speed image sets. (Figure 13 shows a sequence of 10 such instantaneous images.) The inlet conditions were T_3 = 828 K, P_3 = 1034-kPa, and ϕ = 0.35. The average of those images is representative of the steady-state system (and identical in form to those obtained via the ICCD), while the RMS (standard deviation) of those images tells us there is a large variation about the mean, particularly in the region immediately downstream of the fuel injection sites. The third image shows the signal range (signal maximum – signal minimum) and like the RMS, indicates a large variation, but it also serves to point out that variation extends well downstream, where the RMS is low.

We also processed the images in a manner typical for PIV processing. For these images, we are tracking the bulk flame intensity (as represented by C_2^* and CH^* within the flame front) changes over time. The time between images is 100-μs, a relatively long time compared to the 5-μs time between PIV image pairs. However, in observing the play-back of the high speed movies, and in considering that we can track by eye, "movement" from frame to frame (as in the single frames of Figure 13), the time between frames is not too long. It is reasonable that PIV-type processing may provide insights into LDI flame structure, especially since C_2^* and CH^* are indicators of the primary reaction zone. It is also important to keep in mind that each individual image from the high speed camera captures the light emitted throughout the volume of the optically-accessible region and does not isolate individual planes as with PLIF and PIV.

The results are shown in Figure 14, with the combustor operating at 1034-kPa. In the top row are images acquired with an inlet temperature of 828 K and in the bottom row, 617 K. The left column has all injectors evenly-fueled with equivalence ratio of 0.35 for the top image and 0.45 for the bottom image. In the right column, only the center injector is fueled, with ϕ_{loc} = 1.32 for the top and ϕ_{loc} = 1.45 at the bottom. The contour denotes the primary flame zone and the arrows can be interpreted as showing the average direction of motion within the flame zone.

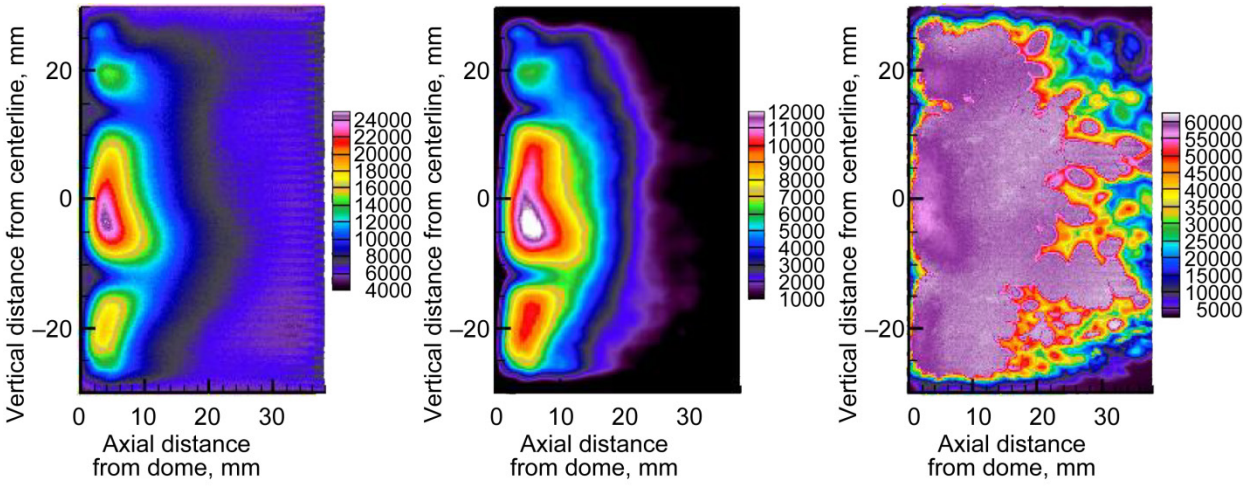

Figure 12.—Statistics derived from processing the signal intensities of 9001 consecutive flame images. Inlet conditions: T_3 = 828 K, P_3 = 1034-kPa, ϕ = 0.35, flow left to right.

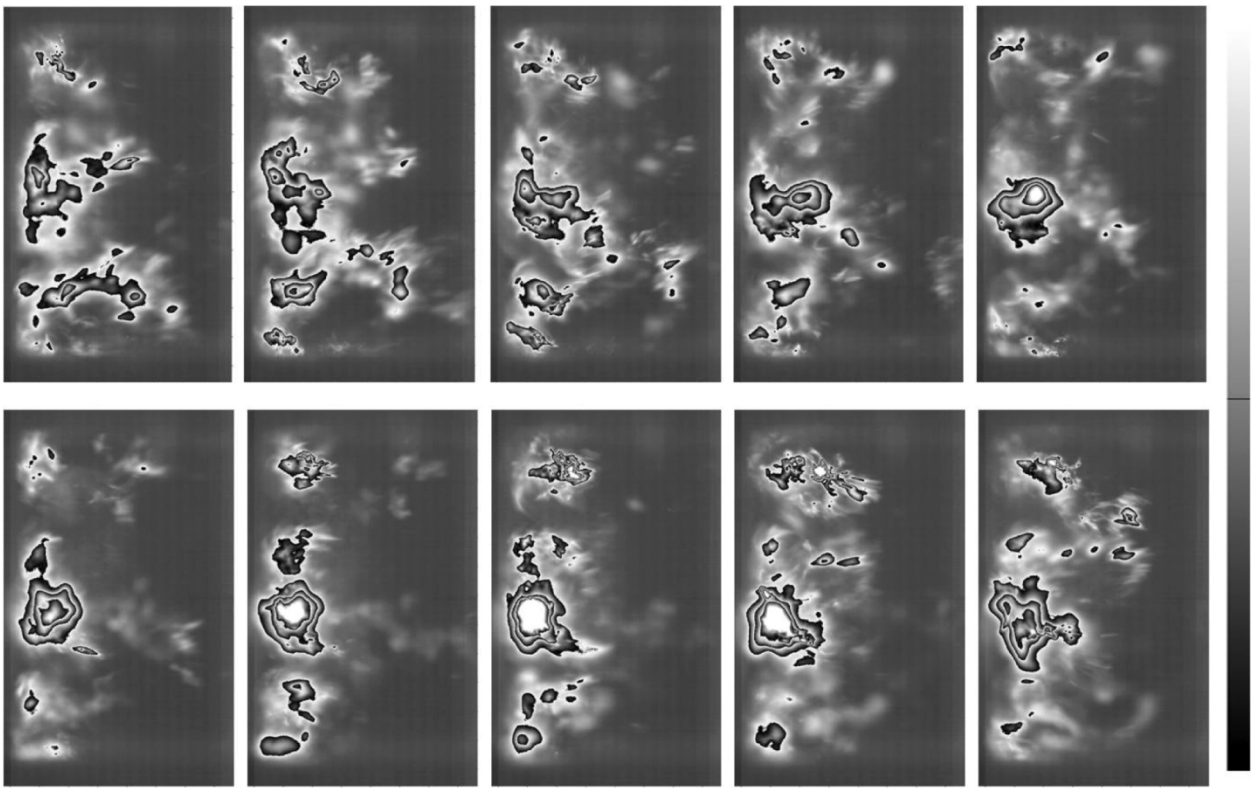

Figure 13.—Ten Consecutive Instantaneous Frames from High Speed Movies, framed at 10 kHz. Inlet conditions: T_3 = 672 K, P_3 = 1034 kPa, ϕ = 0.45. Flow is left to right.

In considering the images of Figure 14 we note the following observations. The high temperature case with all nine injectors fueled is the odd case in terms of the flame visualization observed. It is the only case that does not indicate recirculating eddies within the central core located directly downstream of the fuel injection sites. However, earlier work using phase Doppler interferometry (Ref. 10) indicates a weakened recirculation zone during combustion. The lower temperature, all-fueled case also supports that work because we observe a much shorter recirculation region (Figure 14, lower left). In comparing the center-fueled injector cases to those with all nine injectors, the former show relatively strong recirculation near the dome and a much greater extent of coherent structure much farther downstream, at x = 35-mm. This is commensurate with the flame zone being longer because of the fuel-rich front end. In contrast, the two evenly fueled cases do not show coherent structure beyond x = 20-mm at low temperature and x = 15-mm at high temperature.

It is possible that heat release effectively decreases the swirl number; the decrease in swirl number would lead to decreased flame stability. As the fuel burns, the overall density of the fuel/air mixture decreases. This density decrease leads to an increase in axial velocity because the mass flow rate remains the same. However, it can be argued that the radial velocity remains approximately the same because the radial velocity is imparted to the flow by swirlers that are upstream of the combustion zone. Experiments with swirling jets show that the recirculation zone disappears for low swirl numbers (Ref. 16).

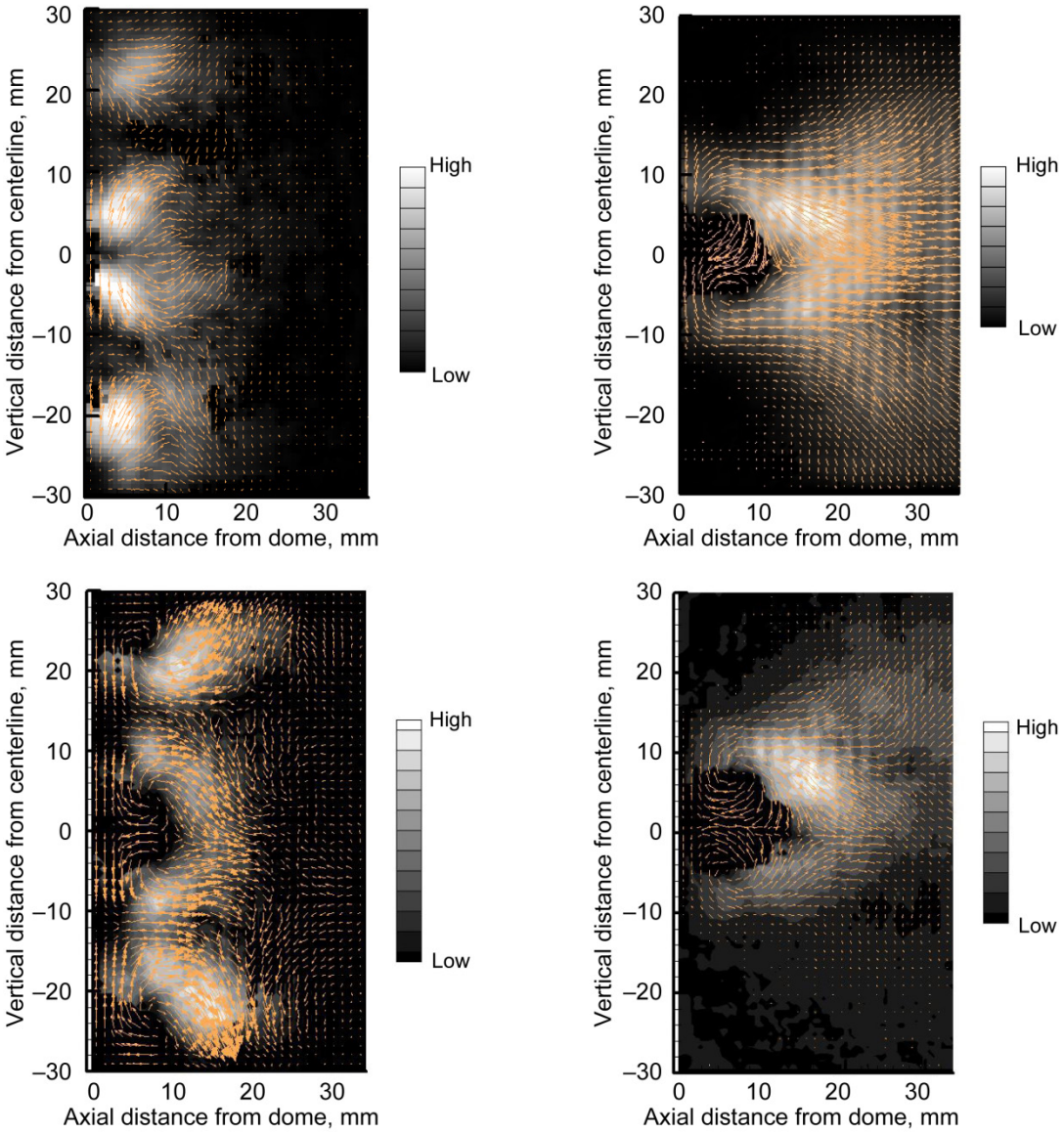

Figure 14.—Average Flame/Flow structure derived using PIV-type processing of 9000 successive high-speed image pairs. Top row: T_3 = 828 K. Bottom row: T_3 = 617 K. Left column: Nine injectors fueled equally. Right column: Center injector fueled only.

Figure 15 serves to help characterize combustion at a single inlet condition using complementary diagnostics techniques: CH^* chemiluminescence, OH and fuel PLIF, and spontaneous Raman spectroscopy. T_3 = 828 K, P_3 = 1034-kPa, and ϕ = 0.35. Key features are that the injector produces a highly symmetric flow field. The fuel PLIF (bottom left) shows that the fuel, as represented by naphthalene-based molecules, is consumed quickly. CH^* (upper left) supports this; CH breakdown/recombination begins immediately at the dump plane, and the primary reaction zone is located there. The plot of OH PLIF (upper right) shows axial, horizontal, and vertical slices from a 3–D data block, highlighting the symmetry, but also showing (along with the CH^*) that little or no interaction occurs between LDI elements. Finally, the SRS (lower right) data provides us with reasonable combustion temperatures 4-mm above the 9-point LDI centerline, and shows that the high temperature regions lie immediately downstream of the injector elements. The SRS data also suggest little interaction, and its form is consistent with 1-point CFD results (Ref. 13).

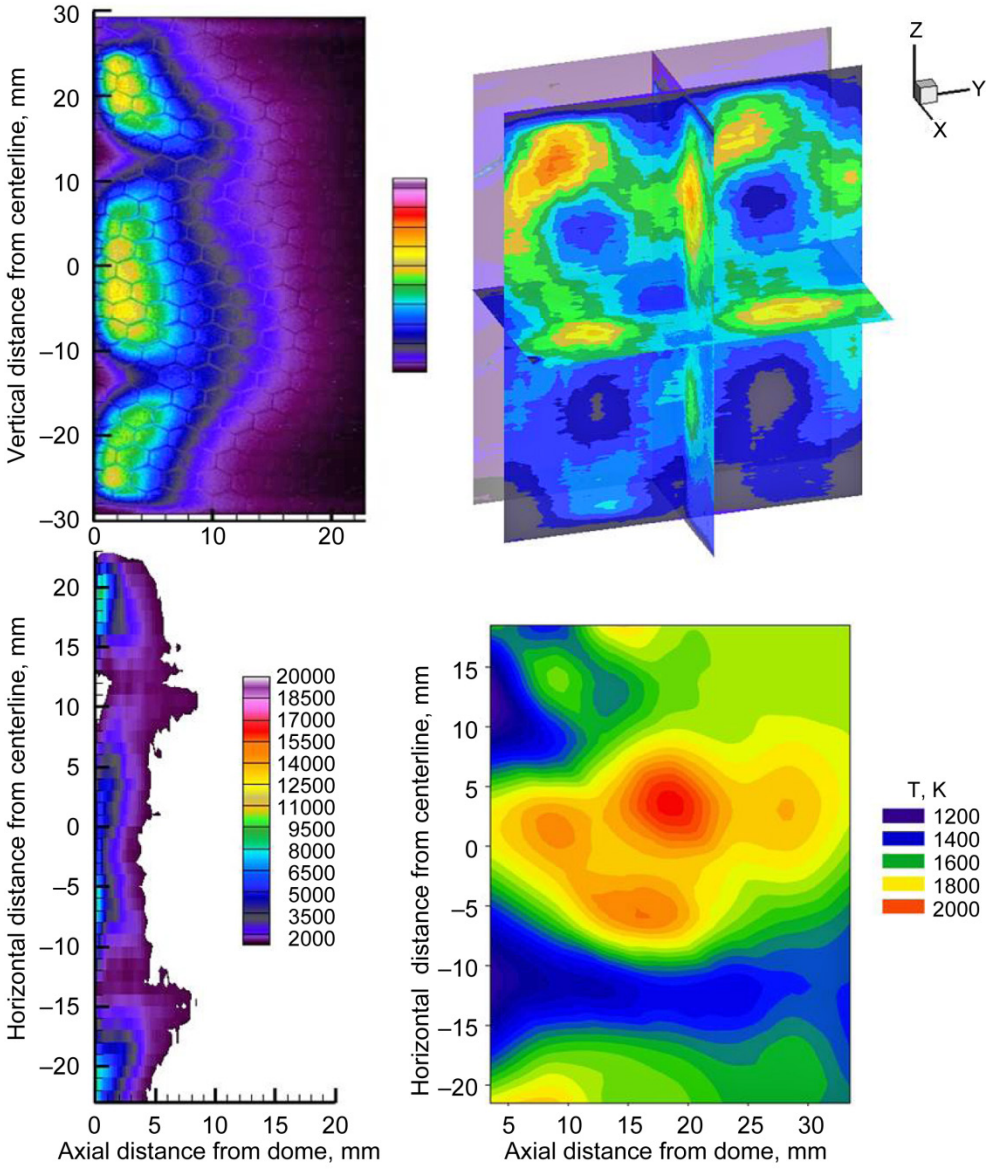

Figure 15.—Results using (top row) CH^* and OH PLIF and (bottom row) Fuel PLIF and SRS at T_3 = 828 K, P_3 = 1034-kPa, and ϕ = 0.35.

Summary

In this paper, we have presented recent measurements taken in an optically-accessible, JP8-fueled, flame tube combustor using baseline nine-element lean direct injection (LDI) research hardware. Extensive measurements were presented for the cases where all elements are evenly fueled and measurements where only the center element is fueled. PIV and chemiluminescence measurements show that the burning zone extends farther downstream for the center-only cases than it does for the corresponding equally-fueled cases; this is consistent with the local equivalence ratio being much higher for the center-only cases than it was for the evenly-fueled cases. Results from the high speed chemiluminescence measurements suggest that combustion reduces the size of the recirculation zone. PLIF, chemiluminescence, and SRS results suggest that the burning results for each element are local and that the interaction between elements is limited.

References

1. U.S. Government Accountability Office. Report to Congressional Committees. "Aviation and Climate Change: Aircraft Emissions Expected to Grow, but Technological and Operations Improvements and Government Policies Can Help Control Emissions," GAO-09-554, 2009.
2. U.S. Congress. Partnership for Air Transportation Noise and Emissions Reduction. "Report to the United States Congress: Aviation and the Environment," 2009. http://web.mit.edu/aeroastro/partner/reports/congrept_aviation_envirn.pdf; Accessed: 4/21/2011.
3. U.S. Federal Aviation Administration, "Aviation & Emissions: A Primer," Office of Environment and Energy, Washington, DC 2005.
4. Johnson, H.S., Kinnison, D.E., Wuebbles, D.J., "Nitrogen Oxides from High Altitude Aircraft: An Update of Potential Effects on Ozone," J. of Geophysical Research, Vol. 94, No. D13, 1989, p. 16,351-16,363.
5. Tacina, R., Lee, P., and Wey, C., "A Lean-Direct-Injection Combustor Using a 9 Point Swirl-Venturi Fuel Injector," ISABE-2005-1106, 2005.
6. Locke, R.J, Hicks, Y.R, and Anderson, R.C., "Combustion Imaging Using Fluorescence and Elastic Scattering," *Optical Metrology for Fluids, Combustion, and Solids*, edited by C. Mercer, Kluwer Academic Publishers, Norwell, MA, 2003, pp. 175-208.
7. Hicks, Y.R., Locke, R.J., and Anderson, R.C., "Optical Measurement and Visualization in High-Pressure, High-Temperature, Aviation Gas Turbine Combustors," *Optical Diagnostics for Industrial Applications*, edited by Neil A. Halliwell, editor, Proceedings of SPIE Vol. 4076, 2000, pp. 66–77. Also published as NASA/TM—2000-210377, 2000.
8. Cai, J., Jeng, S.-M., and Tacina, R., "The Structure of a Swirl-Stabilized Reacting Spray Issued From an Axial Swirler," AIAA-2005-1424, 2005.
9. Hicks,Y.R., Anderson, R.C., and Locke, R.J., "Optical Measurements in a Combustor Using a 9-Point Swirl-Venturi Fuel Injector," International Society for Air Breathing Engines, ISABE-2007-1280, 2007.
10. Heath, C.M., Locke, R.J., Anderson, R.C., and Hicks, Y.R., "Optical Characterization of a Multipoint Lean Direct Injector for Gas Turbine Combustors: Velocity and Fuel Drop Size Measurements," IGTI, GT2010-22960, 2010.
11. Chen, K.-H., Norris, A.T., Quealy, A., and Liu, N.-S., "Benchmark Test Cases for the National Combustion Code," AIAA-1998-3855, 1998.
12. Davoudzadeh, F., Liu, N.-S., Moder, J.P., "Investigations of Swirling Air Flows Generated by Axial Swirlers in a Flame Tube," IGTI, GT-2006-91300, 2006.
13. Iannetti, A.C., and Moder, J.P., "Comparing Spray Characteristics from Reynolds Averaged Navier-Stokes (RANS) National Combustion Code (NCC) Calculations Against Experimental Data for a Turbulent Reacting Flow," AIAA-2010-578, 2010. Also published as NASA/TM—2010-216735, 2010.

14. Iannetti, A., Tacina, R., Jeng, S.-M., and Cai, J., "Towards Accurate Prediction of Turbulent, Three-Dimensional, Recirculating Flows With the NCC," AIAA-2001-0809, 2001. Also published as NASA/TM—2001-210761.
15. Stubbs, R.M., and Liu, N.-S., "Preview of the National Combustion Code," AIAA-97-3114, 1997.
16. Beer, J.M., Chigier, N.A., *Combustion Aerodynamics*, John Wiley and Sons, Inc., New York, 1972.

REPORT DOCUMENTATION PAGE		Form Approved OMB No. 0704-0188

1. REPORT DATE *(DD-MM-YYYY)*	2. REPORT TYPE	3. DATES COVERED *(From - To)*
01-04-2012	Technical Memorandum	

4. TITLE AND SUBTITLE
Investigations of a Combustor Using a 9-Point Swirl-Venturi Fuel Injector: Recent Experimental Results

5a. CONTRACT NUMBER

5b. GRANT NUMBER

5c. PROGRAM ELEMENT NUMBER

6. AUTHOR(S)
Hicks, Yolanda, R.; Heath, Christopher, M.; Anderson, Robert, C.; Tacina, Kathleen, M.

5d. PROJECT NUMBER

5e. TASK NUMBER

5f. WORK UNIT NUMBER
WBS 561581.02.08.03.16.03;
984754.02.07.03.19.03

7. PERFORMING ORGANIZATION NAME(S) AND ADDRESS(ES)
National Aeronautics and Space Administration
John H. Glenn Research Center at Lewis Field
Cleveland, Ohio 44135-3191

8. PERFORMING ORGANIZATION REPORT NUMBER
E-18001

9. SPONSORING/MONITORING AGENCY NAME(S) AND ADDRESS(ES)
National Aeronautics and Space Administration
Washington, DC 20546-0001

10. SPONSORING/MONITOR'S ACRONYM(S)
NASA

11. SPONSORING/MONITORING REPORT NUMBER
NASA/TM-2012-217245

12. DISTRIBUTION/AVAILABILITY STATEMENT
Unclassified-Unlimited
Subject Category: 07
Available electronically at http://www.sti.nasa.gov
This publication is available from the NASA Center for AeroSpace Information, 443-757-5802

13. SUPPLEMENTARY NOTES

14. ABSTRACT
This paper explores recent results obtained during testing in an optically-accessible, JP8-fueled, flame tube combustor using baseline Lean Direct Injection (LDI) research hardware. The baseline LDI geometry has nine fuel/air mixers arranged in a 3 × 3 array. Results from this nine-element array include images of fuel and OH speciation via Planar Laser-Induced Fluorescence (PLIF), which describe fuel spray pattern and reaction zones. Preliminary combustion temperatures derived from Stokes/Anti-Stokes Spontaneous Raman Spectroscopy are also presented. Other results using chemiluminescence from major combustion radicals such as CH* and C2* serve to identify the primary reaction zone, while OH PLIF shows the extent of reaction further downstream. Air and fuel velocities and fuel drop size results are also reported.

15. SUBJECT TERMS
Laser diagnostics; Fuel injection; Combustion

16. SECURITY CLASSIFICATION OF:			17. LIMITATION OF ABSTRACT	18. NUMBER OF PAGES	19a. NAME OF RESPONSIBLE PERSON
a. REPORT	b. ABSTRACT	c. THIS PAGE			STI Help Desk (email:help@sti.nasa.gov)
U	U	U	UU	24	19b. TELEPHONE NUMBER *(include area code)* 443-757-5802